

UC San Diego

UC San Diego Electronic Theses and Dissertations

Title

Development of Quartz Substrate Circuit Boards for nEXO

Permalink

<https://escholarship.org/uc/item/53g3c3sr>

Author

Ahmad, Taiqoor Zareer

Publication Date

2023

Peer reviewed|Thesis/dissertation

UNIVERSITY OF CALIFORNIA SAN DIEGO

Development of Quartz Substrate Circuit Boards for nEXO

A Thesis submitted in partial satisfaction of the requirements
for the degree Master of Science

in

Physics with a Specialization in Materials Physics

by

Taiqoor Ahmad

Committee in charge:

Professor Liang Yang, Chair
Professor Richard Averitt
Professor Kaixuan Ni

The Thesis of Taiqoor Ahmad is approved, and it is acceptable in quality and form for publication on microfilm and electronically.

University of California San Diego

2023

iii

TABLE OF CONTENTS

| | |
|---|------|
| THESIS APPROVAL PAGE..... | iii |
| TABLE OF CONTENTS..... | iv |
| LIST OF FIGURES..... | v |
| LIST OF TABLES..... | vii |
| ABSTRACT OF THE THESIS..... | viii |
| INTRODUCTION..... | 1 |
| Chapter 1 FABRICATION METHODS AND SAMPLE PREPARATION..... | 5 |
| Chapter 2 TESTING AND METHODOLOGY..... | 9 |
| Section 2.1 ADHESIVE ATTACHMENT..... | 9 |
| Section 2.2 THERMAL CYCLING..... | 12 |
| Chapter 3 RESULTS AND DISCUSSION..... | 13 |
| Section 3.1 INITIAL MEASUREMENTS..... | 14 |
| Section 3.2 ADHESIVE ATTACHMENT RESULTS..... | 15 |
| Section 3.3 THERMAL CYCLING RESULTS..... | 19 |
| Section 3.4 SAMPLE 3 AND 4 RESULTS..... | 25 |
| CONCLUSIONS..... | 32 |
| REFERENCES..... | 34 |

LIST OF FIGURES

Figure 0.1: Cross-section view of the large components of the system outside the TPC, as presented in “nEXO: Neutrinoless double beta decay search beyond 1028 year half-life sensitivity” by Adhikari et. al 2

Figure 1.1: Schematic diagram of the initial paired trace test circuit (top left). The deposited traces are in blue, the substrate dimensions are outlined in red. Actual microfabricated sample 2 after round of silver epoxy thermal cyclic testing (top right). Schematic diagram of the final paired trace test circuit (bottom left)..... 6

Figure 1.2: All samples manufactured at the time of writing. They are, as labeled: A) Sample 1S B) Sample 1L C) Sample 2S D) Sample 2L E) Sample 3 F) Sample 4..... 7

Figure 1.3: The numbering of each trace pair on sample 3 (left) and sample 4 (right) . Each individual trace in the pair is labeled with L or R based on whether it is the left or right trace of that pair in this orientation i.e. pair 13 has traces 13L and 13R. Pairs 11, 21, and 31 on sample 4 are visibly damaged, as is the ground plane visible behind pairs 11, 12, and 13. 8

Figure 2.1: Sample 1L with the two leads attached with silver epoxy. The smooth surfaces of the remaining test pads are clearly visible here, which will be valuable for comparison once thermal cycling has been performed. Right to left, the four rightmost traces are numbered 1, 2, 3, and 4. Traces 1 and 2 have epoxy, 3 and 4 do not. 10

Figure 2.2: Sample 3 with epoxy applied over the corners of the test pads of pairs 12, 23, and 33 and in the center of the test pads of pairs 13, 14, 24, and 34 (left). Sample 4 with epoxy applied over the corners of the test pads of pairs 14, 22, and 32, and in the center of the test pads of 21R, 31R, and pairs 12, 13, and the top pads of pair 32 shorted together (right)..... 11

Figure 3.1: Sample 4, with both the damage behind pairs 11, 12, and 13, and the damage to pairs 11, 21, and 31 clearly visible. Trace 31R is still visibly intact, while trace 21R is present, but discontinuous. 13

Figure 3.2: Sample 2S after the attachment of the 16 gauge copper wire using cuprate solder. The melting of the top copper layer is clearly visible in this image, as is the distinct beaded structure of the solder..... 16

Figure 3.3: Sample 2S after the attachment of the 16 gauge copper wire using silver epoxy after one liquid nitrogen dunk cycle. Note the epoxy with no attached wires or leads on the bottom-leftmost test pad. 17

Figure 3.4: Pair 14 (left) and pair 34 (right) on sample 3. Note the lack of attached leads on the top two test pads of pair 14 and the bottom test pad of trace 34L. 18

Figure 3.5 Oxidized epoxy visible on sample 3 (left) and sample 4 (right). The oxidized epoxy traces can be identified by their yellow coloration as compared to the normal silver coloration of the epoxy..... 18

Figure 3.6: Sample 2S after six thermal cycles (bottom) and the 16 gauge copper wire coated in silver epoxy broken away (top). The copper visible on the bottom of the wire corresponds to visible blemishes in the trace below: Copper was apparently pulled off of the surface by the silver epoxy..... 19

Figure 3.7: The solder test pads of sample 2S after one thermal cycle. Visibly, the opaque copper top layer has been pulled away while the translucent chromium thin interlayer is still present... 20

Figure 3.8: The tape applied to sample 1S. To the left of the 16 gauge white wire are control pads, measured only before and after all cycles. To the right are test pads, measured between every cycle. From left to right, they are numbered 1, 2, 3, 4, with traces 1 and 2 forming one pair, and 3 and 4 forming another. 20

Figure 3.9: The resistance values of Sample 1S's four test traces..... 21

Figure 3.10 The surviving control trace (left) and test traces (right) of sample 1S after thermal cycling..... 22

Figure 3.11: The resistance values of sample 1L's four test traces as labeled in Fig. 2.1 22

Figure 3.12: Sample 1L after all thermal cycling tests. The large damaged sections of copper are visible on traces 1 and 2 to the left. Traces 3 and 4, as well as all of the control traces, had small but visible gaps in the test pads compared to before any tests as seen in figure 2.1. 24

Figure 3.13: Examples of peeled away traces partway through the stress tests of sample 3 (left) and 4 (right) after the first thermal cycle. 28

LIST OF TABLES

| | |
|---|----|
| Table 3-1: The resistances in ohms of all pairs on sample 3. The topmost row in each table labels the column number while the leftmost row labels the row number. There are two entries for each row/column pairing, corresponding to the left and right trace of each pair..... | 14 |
| Table 3-2 The resistances in ohms of all pairs on sample 4. The notations are the same as in Table 3-1. | 14 |
| Table 3-3: The resistances in ohms of all test pairs on sample 3 after the application of silver epoxy and heat treatment at 100°C. The notations are the same as in Table 3-1. CTRL corresponds to control traces that were not measured between thermal cycles. Numbers in bold correspond to test traces without any epoxy. | 25 |
| Table 3-4: The resistances in ohms of all test pairs on sample 4 after the application of silver epoxy and heat treatment at 100°C. The notations are the same as in Tables 3-1 and 3-3. | 26 |
| Table 3-5: The resistances in ohms of all test pairs on sample 3 after the first thermal cycle. The notations are the same as in Tables 3-1 and 3-3. Numbers highlighted in yellow correspond to traces with removed epoxy. | 29 |
| Table 3-6: The resistances in ohms of test pairs on sample 4 after the first thermal cycle. The notations are the same as in Tables 3-1, 3-3, and 3-5. OL (D) corresponds to traces that became discontinuous due to physical damage..... | 29 |
| Table 3-7: The resistances in ohms of all test pairs on sample 3 after the second thermal cycle. The notations are the same as in Tables 3-1, 3-3, 3-5, and 3-6. | 30 |
| Table 3-8: The resistances in ohms of all test pairs on sample 4 after the second thermal cycle. The notations are the same as in Tables 3-1, 3-3, 3-5, and 3-6. | 30 |

ABSTRACT OF THE THESIS

Development of Quartz Substrate Circuit Boards for nEXO

by

Taiqoor Ahmad

Master of Science in Physics with a Specialization in Materials Physics

University of California San Diego, 2023

Professor Liang Yang, Chair

In this paper, various methods were tested to facilitate the creation of copper-based printed circuit boards manufactured on a SiO_2 quartz substrate for use in low-temperature and low-background applications as part of the nEXO collaboration. This technology will be employed for front-end circuitry within the nEXO machinery for the purposes of maximizing the experiment's sensitivity and being able to identify and measure neutrinoless double beta decay.

To identify failure modes, samples were fabricated, characterized, then stress tested mechanically and through submersion into liquid nitrogen. Further samples were thermally cycled between room temperature and -100°C . Thermal cycling was conducted across two metallization schemes: 100 nm copper directly on quartz and 100nm copper deposited onto a 10nm chromium interlayer, which itself was deposited onto quartz. As a result, the Cu-SiO_2 interface was demonstrated to be physically weak, both in terms of its ability to maintain a bond across thermal cycles and its tendency to be easily scraped and damaged by any significant physical pressure. In contrast, the system with a chromium interlayer exhibited much greater physical resilience, with far fewer cases of damage to the traces themselves. In the absence of physical damage and extreme strain, both sets of samples were observed to have stable resistance values. However, the resistances of all copper traces are substantially higher than the theoretical values of bulk copper, and the chromium interlayer has a nontrivial rate of failure. Thus, more research will be needed to identify the best interlayer for use in this circuitry.

INTRODUCTION

From over 30 institutions across the world, particle physicists and instrumentation specialists are coming together to form the nEXO collaboration, with the mission of isolating and observing neutrinoless double beta decay ($0\nu\beta\beta$). If successfully observed and studied, $0\nu\beta\beta$ could open the door to physics beyond the standard model by providing evidence of a violation of lepton number conservation, possibly helping us understand the baryon asymmetry observed in our universe. A successful measurement of the $0\nu\beta\beta$ half life would also help set upper bounds to the Majorana mass of the neutrinos involved.

Liquid ^{136}Xe (LXe) is an attractive particle to study for this due to its high Q-value of its double β decay relative to other natural decay processes. Since it's a noble gas, Xe can also be made pure of radioactive contaminants relatively easily. The abundant ^{136}Xe isotope can also be isolated at relatively low cost, meaning that a multi-ton system holding LXe in a time-projection chamber (TPC) is both practical and useful, with a $0\nu\beta\beta$ decay half-life of over 3.5×10^{25} years as measured in the previous EXO-200 experiment. The current nEXO collaboration aims to go beyond this and reach 10^{28} year half-life sensitivity (Adhikari et. al., 2021).

The nEXO conceptual design as shown in figure 0.1 involves a copper TPC vessel containing five tons of liquid Xenon, with a cathode beneath the chamber, field-shaping coils surrounding it, and an anode of crossed electrode strips forming uniform readout tiles above it. Surrounding the TPC is an HFE coolant vessel that both regulates the temperature and isolates outside interference, and beyond that is a vacuum chamber which provides thermal insulation between the inner vessel and an outer vessel containing a water shield. Thus, the TPC is isolated from the outside due to the incredibly high sensitivity needed. This sensitivity also requires that the front end circuitry be established inside the inner vessel to minimize electronic noise.

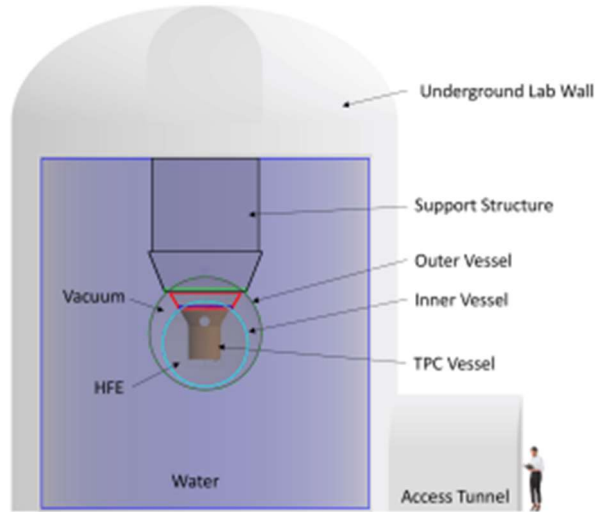


Figure 0.1: Cross-section view of the large components of the system outside the TPC, as presented in “nEXO: Neutrinoless double beta decay search beyond 1028 year half-life sensitivity” by Adhikari et. al

Conventional printed circuit boards such as FR4 contain too much radioactive contamination and cannot be placed directly in the detector. To address this issue, low-background materials are being investigated for use in the printed circuit boards (PCBs) in the system. Of particular interest for the PCBs are fused silica quartz as a substrate and copper as the primary means of metallization, as they can be produced with extremely low background.

Copper forms the ideal metallization in any low-background application due to its extremely low incidence of radioactive isotopes, as identified via inductively-coupled plasma mass spectroscopy by the Majorana Demonstrator Radioassay program. Using Thorium-232 as a benchmark isotope due to its consistent responses within the Radioassay study, electroformed copper was found to have levels on the order of 10^{-14} grams per gram of copper. In comparison, fused silica quartz had levels on the order of 10^{-10} g per gram of quartz. Other materials of interest included Sn-Ag-based solder, with ^{232}Th levels on the order of 10^{-11} g/g, silver epoxy, with counts similar to those of quartz, and sputtered Cr, with the highest incidence rate on the order of 10^{-9} g/g (Abgrall et. al., 2016).

With this in mind, I developed the parameters for this experiment: To identify the feasibility to manufacture and employ low-background circuitry, the adhesive and electronic properties of Cu and SiO₂ quartz will be examined. However, the adhesion of these two materials is notably poor, particularly as temperatures approach the boiling point of Xenon and below, as is the case in the LXE environment in the nEXO experiment's TPC.

One of the likely causes of this low adhesion is the variable interfacial bond strength between copper and amorphous quartz. In studies on crystalline SiO₂, the bond strength was found to be directly proportional to the surface oxygen density of the silica. For most types of surface bonds, namely Cu-Si and Cu-O bonds, the interface becomes a weak link, where stress-based fractures begin and expand throughout the interface. Only in Cu-OO bonds does the fracture occur within the Cu lattice rather than at the interface. Without any way of ensuring a consistently high concentration of surface oxygen, the Cu-SiO₂ interface becomes a major weak point for the system (Shan et. al., 2011).

Macroscopically, lateral displacement between copper thin films and SiO₂ substrates has been observed, where the copper detaches entirely from the substrate surface at a displacement of 3.2nm (Cui et. al., 2018). This displacement can be engaged easily through thermal expansion and contraction of copper where in contact with silicon or SiO₂, leading to the formation and propagation of interfacial cracks (Fei et. al., 2020).

The most common way to circumnavigate this issue of poor adhesion between copper and SiO₂ is to deposit a more adhesive interlayer that can disperse thermal stresses between the Cu layer and the quartz substrate (Yang et. al. 2023). One of the most common materials that sees use in this way is chromium, as its presence spontaneously breaks surface SiO bonds in the silica, allowing for a much stronger bond with the oxygen in the quartz (Baima et. al. 2020).

Thus, the work I set out to accomplish in this study was to confirm the expected adhesiveness results and measure trace integrity across both Cu-Cr-SiO₂ and Cu-SiO₂ samples. The nEXO collaboration's needs involve systems that must be cooled to the boiling point of Xenon, and thus to those ends, the traces fabricated for this study would be thermally cycled at high intensities through liquid nitrogen submersion and low intensities through a controlled environment chamber. The end goal was to identify the feasibility for these types of circuits for use in nEXO front-end circuitry.

In order to control applied power, deposition time, deposition pressure, and trace thickness, as well as to quickly and easily manufacture samples with a variety of trace patterns and a variety of metallizations, traces were fabricated locally through UCSD's Nano3 facility.

Chapter 1 FABRICATION METHODS AND SAMPLE PREPARATION

The substrates to be investigated here are thin transparent quartz square wafers with 76mm. length and width and a thickness of 300 microns. For the traces, regardless of material, the target width of interest ranges from 0.6mm to 1mm, while the target thickness is around 100nm. With these dimensions in mind, the current nEXO specifications involve electroformed copper deposited directly onto the substrate.

Though the local microfabrication facility Nano3 at UCSD did not have any means of electroforming copper, because the process is primarily used to mitigate backgrounds, we instead chose to use the existing lithography and sputtering systems offered by the facility for ease of manufacturing and testing of the prototypes physically and electronically.

In the Nano3 cleanroom, the wafers were first cleaned through 10 minutes of ultrasonic agitation each in acetone, ethanol, and 70% isopropyl alcohol before being rinsed with deionized water and dehydration baked at 180°C for 10 minutes. Following this, AZ 12XT-20PL-5 positive spin-on photoresist was applied with the procedure provided by the Nano3 facility. The photoresist was then exposed with the desired circuit pattern in a Heidelberg MLA 150 laser writer at 375nm with a dose of 500mJ/cm². Then, in a solution of AZ300 MIF developer, the exposed photoresist was removed, leaving behind the desired circuit pattern shown in figure 1.1.

Regarding the metallization process, all material deposition was performed in a Denton Discovery 635 sputtering machine under an Ar gas flow in the Nano3 cleanroom. For all samples, copper was sputtered at 200W with a pressure of 3.1mT for 3 minutes for an expected layer thickness of 100nm. For the samples with chromium interlayers, Cr was sputtered at 50W with a pressure of 12.9 mT for 3.5 minutes for an expected layer thickness of 5-7nm.

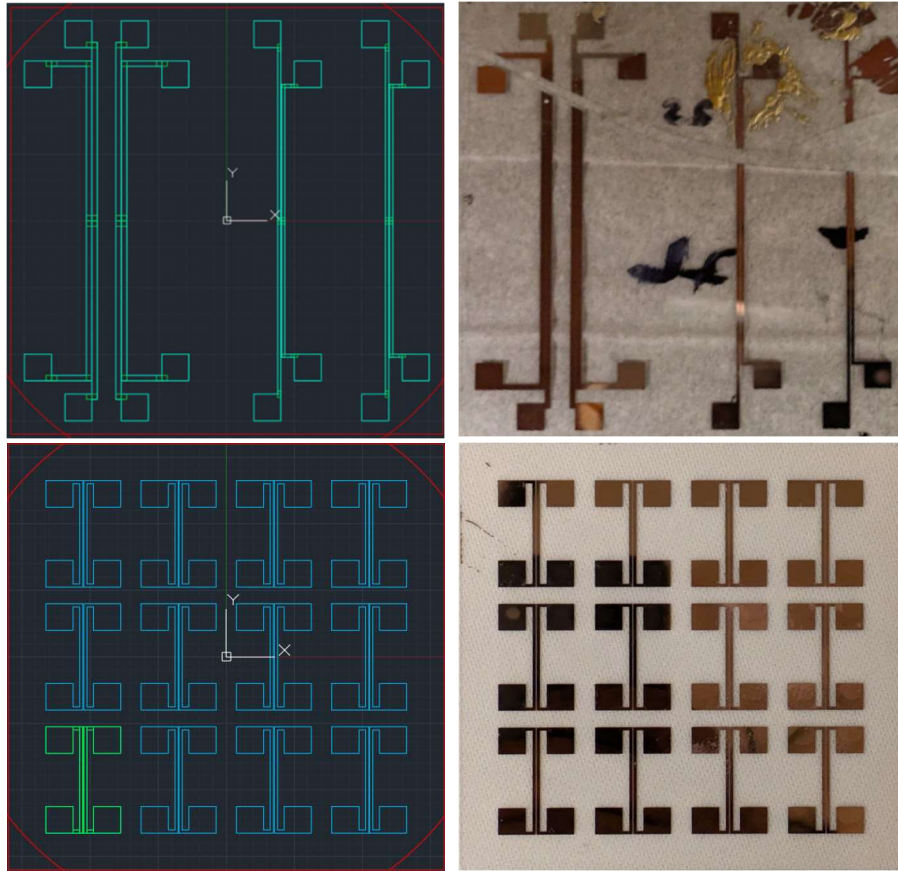


Figure 1.1: Schematic diagram of the initial paired trace test circuit (top left). The deposited traces are in blue, the substrate dimensions are outlined in red. Actual microfabricated sample 2 after round of silver epoxy thermal cyclic testing (top right). Schematic diagram of the final paired trace test circuit (bottom left). The final deposited traces are in blue, the target deposition zone is outlined in red. Actual microfabricated sample 3 (bottom right).

As the final step, the test circuits were left from 2-4 days in a remover PG solution to dissolve the photoresist and lift off all unwanted depositions, leaving behind only the desired traces. Afterwards, the samples were sonicated first in a fresh remover PG solution, then in deionized water to ensure only clean traces remained. In the first set of fabricated circuits, both samples were broken at this final step when subject to being rinsed with deionized water through a spray gun to clean any remaining remover PG or loose metal. To avoid this, all further samples were rinsed in a low-intensity stream of deionized water for the final clean instead of being sprayed with it at relatively high pressure.

Instead of being discarded, the broken samples were used as low-risk tests of the experimental setup. These broken samples were labeled based on size and the larger wafer of origin. One wafer had traces of higher visual fidelity, and thus was designated wafer 1. The other wafer had visual indications of imperfections in the deposited copper, and was designated wafer 2. Each fragment of the two wafers was labeled with a letter: S for the small half, and L for the large half. In this way, the four fragments were prepared as 1S, 2S, 1L, and 2L (Fig. 1.2).

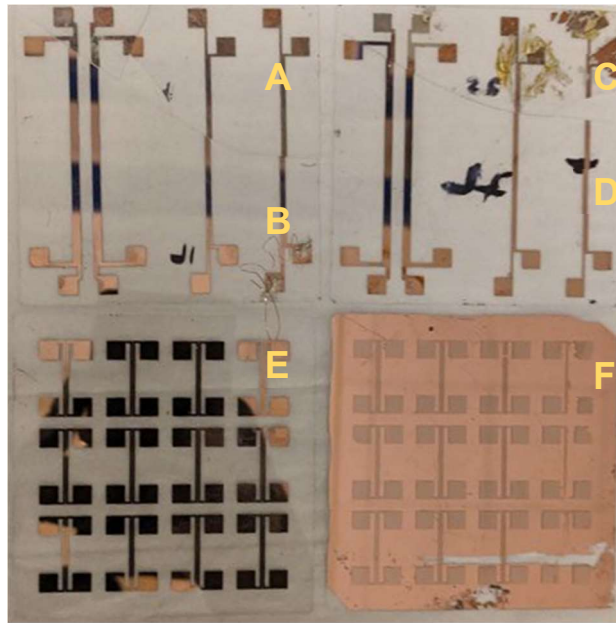


Figure 1.2: All samples manufactured at the time of writing. They are, as labeled: A) Sample 1S B) Sample 1L C) Sample 2S D) Sample 2L E) Sample 3 F) Sample 4

Once wafers 1 and 2 were broken, two more were fabricated based on a pattern of uniform trace widths of 0.6mm and gap widths of 0.15mm, with shorter pairs allowing for twelve distinct testable pairs on a single wafer (Fig. 1.1). One of these was fabricated with a chromium interlayer as with wafers 1 and 2. This will be designated sample 3. The other was fabricated with pure copper on quartz, with a ground plane on its back side that was deposited by accident. This will be designated sample 4 (Fig. 1.2). Due to the large number of paired traces present in samples 3 and 4, each pair has been numbered based on its row and column (Fig. 1.3).

In the final cleaning and lift-off step, all samples were subject to ultrasonic agitation twice. In this step, all samples were supported on one end by a small number of glass slides to prevent them from forming a watertight seal as they lay flat in the beaker. For samples 1, 2, and 3, this caused no issues. For sample 4, the only sample with copper directly being deposited onto quartz, this led to visible damage as copper was peeled away from the substrate. This damage was observed both when sonicated face-up and face-down. The face-up sonication caused the ground plane on the back of sample 4 to be damaged in a straight line behind pairs 11, 12, and 13, while the face-down sonication caused pairs 11, 21, and 31 to be partially peeled away from the circuit (Fig. 1.3).

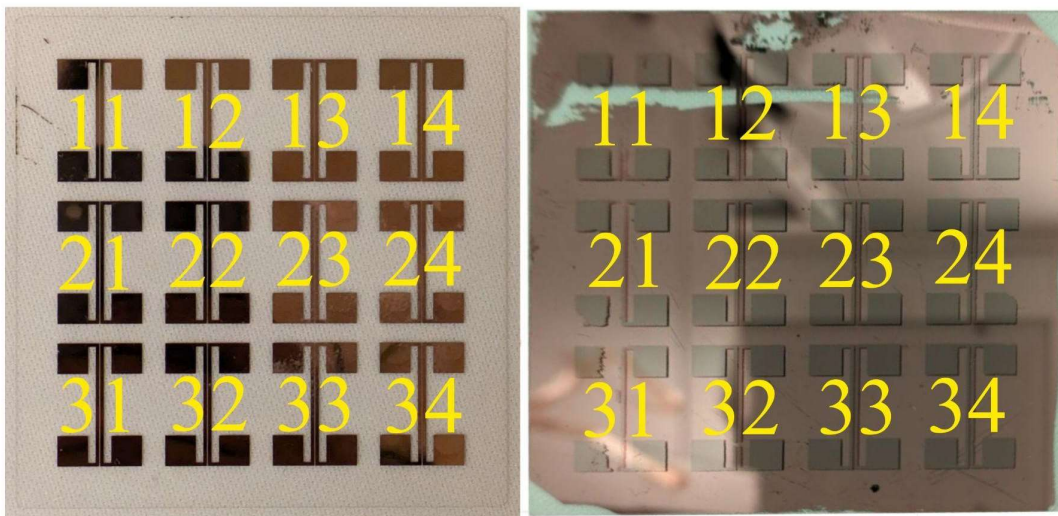


Figure 1.3: The numbering of each trace pair on sample 3 (left) and sample 4 (right) . Each individual trace in the pair is labeled with L or R based on whether it is the left or right trace of that pair in this orientation i.e. pair 13 has traces 13L and 13R. Pairs 11, 21, and 31 on sample 4 are visibly damaged, as is the ground plane visible behind pairs 11, 12, and 13.

Chapter 2 TESTING AND METHODOLOGY

Initially, the resistances of all traces, across all fragments of samples 1 and 2 and across both samples 3 and 4, were measured using a Fluke 115 True RMS Digital Multimeter to confirm the successful fabrication of each trace. To test the viability of various methods of attaching leads to the circuit for the purposes of consistently testing impedance at cryogenic temperatures, 16 gauge stranded copper wire was attached to the clean traces of samples 1S and 2S using Austor Sn, 0.3-Ag, 0.7-Cu solder and AA-Duct 907 conducting silver epoxy. These leads were tested in a variety of manners. The results of all tests mentioned above and below will be presented and discussed in the Results section.

Section 2.1 ADHESIVE ATTACHMENT

First, a soldering iron was applied directly to the deposited copper trace on sample 2S in intervals of roughly 10°C from around 38°C to around 200°C to test the copper thin film's resistance to temperatures within the range of interest for various solders. Then, the Austor solder was applied to the same sample at 200°C. With another trace on sample 2S, the Austor solder was applied without any initial heat tests to control the damage to the trace before the solder was applied.

Regarding the silver epoxy, first a 16 gauge stranded copper wire was attached to sample 2S with an excess of silver epoxy to establish a connection. This was done by first lathering silver epoxy on the surface, then splaying the wires inside the lead outwards to maximize surface area and placing them on the lathered epoxy using a soldering stand with alligator clips, leading to the completion of one test trace and a number of miscellaneous traces used for a variety of preliminary tests, as will be discussed later.

Later, on sample 1L, individual strands from the same copper wire were extracted, and a smaller amount of silver epoxy was used to bind them to two of the test pads. In this case, the strands were positioned via alligator clips beforehand, and then silver epoxy was applied carefully to prevent any shorting between the pairs. Leads were attached via epoxy to the rightmost pair as an epoxy test pair, with the adjacent pair being left as a zero-epoxy test pair, and the leftmost two pairs being measured only at the very beginning and end of the process as a set of control pairs (Fig. 2.1).

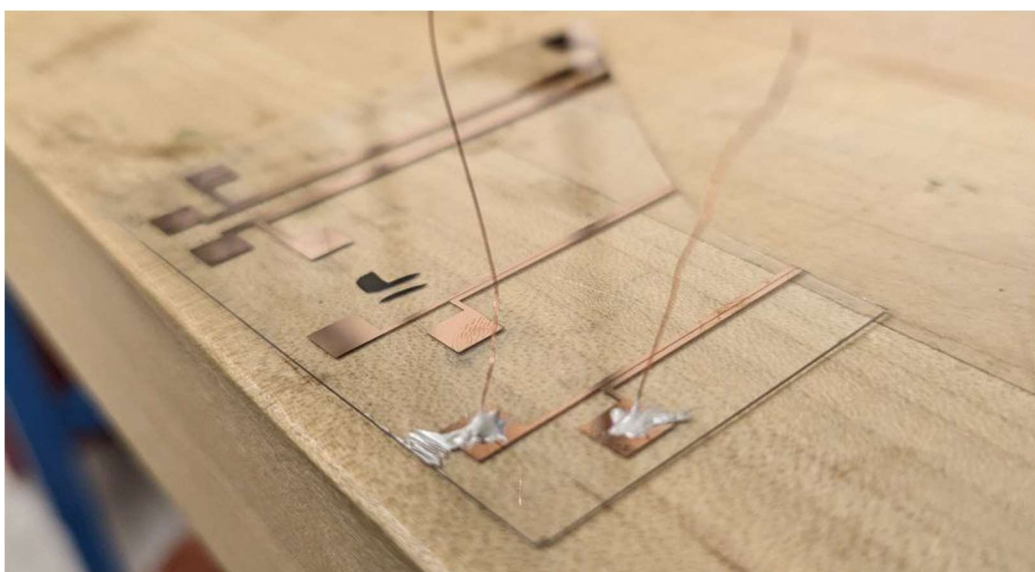


Figure 2.1: Sample 1L with the two leads attached with silver epoxy. The smooth surfaces of the remaining test pads are clearly visible here, which will be valuable for comparison once thermal cycling has been performed. Right to left, the four rightmost traces are numbered 1, 2, 3, and 4. Traces 1 and 2 have epoxy, 3 and 4 do not.

For sample 3, single-strand leads were attached via epoxy to pairs 14 and 34. For these, a single strand was attached to each test pad, leading to eight leads in total across the two pairs. These were attached by holding four strands within a single alligator clip, contorting each strand to press against one of the test pads, then applying a small amount of silver epoxy where the two meet. However, due to difficulties maintaining individual strand integrity and complications in measurements, these would be the final individual strands to be attached to the samples.

Instead, to isolate the effect of silver epoxy, a small amount of the substance was dabbed onto the test pads of pairs 34 and 33 on sample 3, as well as pairs 12, 13, and individual traces 21R and 31R on sample 4. Additionally, as both traces in pair 32 on sample 4 are discontinuous near the lower test pads, they were shorted together using silver epoxy to form an additional testing surface. Finally, pairs 12, 23, and 33 on sample 3 and pairs 14, 22, and 23 on sample 4 had epoxy applied to the corners of each test pad to test its adhesion with the SiO₂ substrate as well as strain that may arise due to bonds between both materials (Fig. 2.2).

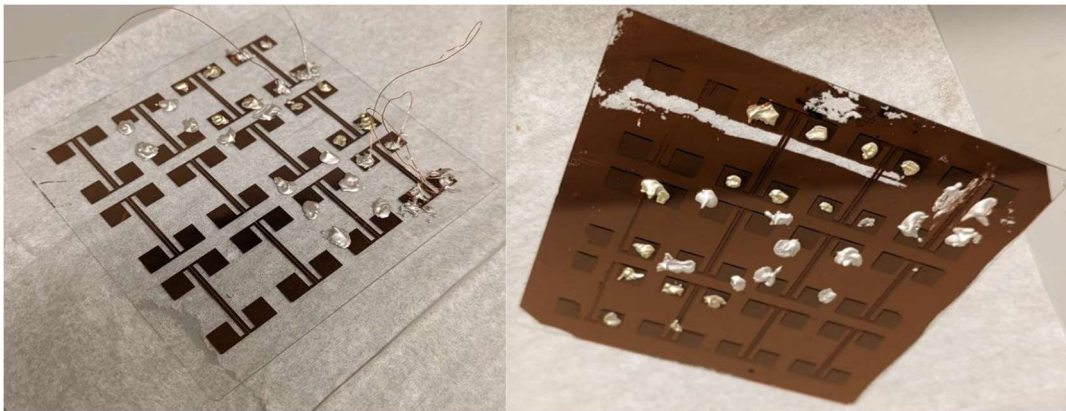


Figure 2.2: Sample 3 with epoxy applied over the corners of the test pads of pairs 12, 23, and 33 and in the center of the test pads of pairs 13, 14, 24, and 34 (left). Sample 4 with epoxy applied over the corners of the test pads of pairs 14, 22, and 32, and in the center of the test pads of 21R, 31R, and pairs 12, 13, and the top pads of pair 32 shorted together (right).

Resistance measurements were initially performed on both adhesive methods once a connection was apparently made. For initial measurements on fragments of samples 1 and 2, this was done by holding one lead of the multimeter to the attached wire or single-strand lead, and touching the other lead to the thin end of the fragment's trace. For samples 3 and 4, this was done using the epoxy or leads attached to each test pad. Once a connection was confirmed, each bond was then stress tested by gently tugging on each exposed lead. Given that they succeeded in the stress test, they were then tested through a process of thermal cycling.

Section 2.2 THERMAL CYCLING

Samples 1S and 2S were tested by being submerged into liquid nitrogen (LN). Sample 2S was suspended in this process by the lead attached to it by silver epoxy. Sample 1S was suspended by a wire attached to its back side by tape. Both samples were quickly lowered into LN until completely submerged. They were then left in until the LN stopped boiling to ensure they reach thermal equilibrium with LN. The samples were then lifted out of the LN and allowed to return to room temperature. Sample 2S was only investigated for mechanical failure in the silver epoxy it was being held by. Sample 1S was measured between each submersion for the resistance of each test trace. Each sample detached from its lead after six thermal cycles.

After these tests, samples 1L, 3, and 4 were thermally cycled within a more gentle Sun Systems EC1X model controlled environment chamber, which cooled them down to -100°C over the course of fifteen minutes. The samples were then held at this temperature for ten minutes before being brought back to room temperature over an additional fifteen minutes. For sample 1L, resistance was taken across the two test pairs between every cycle, while the control pairs were only measured once before any cycles and once when the thermal cycling was concluded. For samples 3 and 4, all traces with epoxy present were tested between each cycle both using a set of tweezers to try to pull away the epoxy and for resistance via the multimeter. For sample 3, pairs 22 and 32 were measured between every cycle while all pairs in column 1 were measured only before and after all cycles. For sample 4, pair 33 was measured between every cycle while pairs 24 and 34 were only measured before and after all cycles. This was done to control for both the degradation of the copper trace across thermal cycles and the mechanical strain of the multimeter scraping copper away between every cycle.

Chapter 3 RESULTS AND DISCUSSION

Before any tests were performed on the test samples, the process of fabricating them already indicated a number of properties that are of note for the purposes of this study, both with regards to the fabrication itself and the resultant resistances initially measured across the different traces on each sample.

As mentioned above in the fabrication methods, the ultrasonic agitation of sample 4 led to copper being easily peeled away from the substrate on both sides (Fig. 3.1). This was a behavior not observed in samples 1, 2, and 3, all of which have chromium interlayers between the copper and the quartz as an adhesive aid. This indicates that even without thermal cycling or any topical adhesives such as solder or epoxy, copper already has a low adhesiveness to SiO₂ quartz.

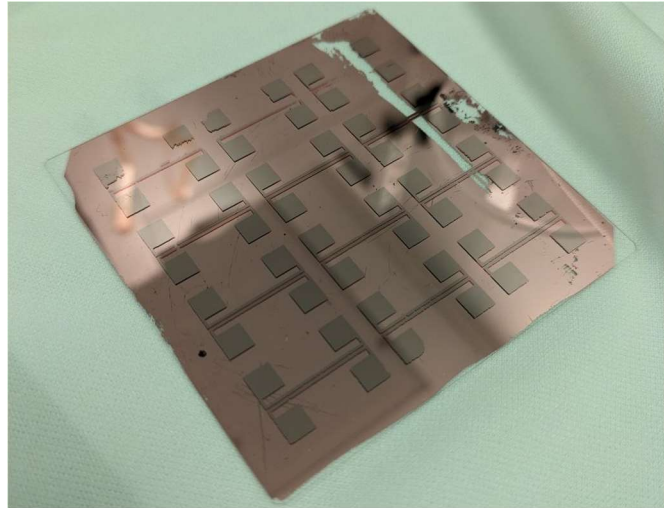


Figure 3.1: Sample 4, with both the damage behind pairs 11, 12, and 13, and the damage to pairs 11, 21, and 31 clearly visible. Trace 31R is still visibly intact, while trace 21R is present, but discontinuous.

Section 3.1 INITIAL MEASUREMENTS

Initial resistance measurements taken of the copper traces on all samples yielded consistent yet unexpected results. Because the broken fragmented samples 1 and 2 have traces of variable width and quality due to the breakage, the initial resistance measurements of samples 3 and 4 are more useful and thus are the primary measurements being presented here. These values were obtained by taking resistance measurements across multiple points on both testing pads, then taking the sample average and standard deviation to identify the resistance across the entirety of both test pads.

Table 3-1: The resistances in ohms of all pairs on sample 3. The topmost row in each table labels the column number while the leftmost row labels the row number. There are two entries for each row/column pairing, corresponding to the left and right trace of each pair. OL corresponds to discontinuous traces. Underlined values correspond to traces with rapidly fluctuating resistance values, and thus have a limited degree of accuracy.

| S. 3 | 1 | | 2 | | 3 | | 4 | |
|------|----------|----------|----------|-----------------|-----------------|----------|----------|----------|
| 1 | 23.5±1.5 | 23.4±2.0 | 23.4±1.8 | 23.6±1.4 | OL | 24.4±2.6 | 24.6±3.0 | 24.3±2.1 |
| 2 | 23.5±1.8 | 24.1±2.1 | 24.7±1.5 | <u>24.5±1.4</u> | <u>24.6±1.4</u> | 24.5±1.9 | 24.7±1.8 | 25.0±2.3 |
| 3 | 23.0±1.7 | 23.4±1.6 | 23.3±1.3 | 23.0±1.7 | <u>23.9±1.6</u> | 23.5±1.6 | 24.4±1.4 | 25.4±1.3 |

Table 3-2 The resistances in ohms of all pairs on sample 4. The notations are the same as in Table 3-1.

| S. 4 | 1 | | 2 | | 3 | | 4 | |
|------|----|----------|----------|----------|-----------------|-----------------|----------|----------|
| 1 | OL | OL | 26.6±1.3 | 27.0±1.9 | 31.7±2.2 | 31.0±1.3 | 31.2±2.0 | 31.5±2.6 |
| 2 | OL | OL | 25.4±2.2 | 25.4±1.6 | 30.8±2.5 | <u>30.6±1.3</u> | 29.5±2.1 | 30.8±1.4 |
| 3 | OL | 45.1±1.2 | OL | OL | <u>28.8±2.4</u> | 28.9±2.8 | 30.2±2.1 | 30.3±1.4 |

The resistance values listed for samples 3 and 4 here match an unexpected trend across resistances of all traces on all samples and fragments: For a copper trace at room temperature around 22mm in length, 0.6mm in width, and 100nm in thickness, the expected resistance is around 6Ω. At the furthest edges of the test pads, this increases to around 8Ω. Thus, at the

absolute best conditions, the experimental resistances obtained for sample 3, around 24Ω , are about three times greater than expected (Table 3-1).

A likely mechanism for this discrepancy lies in the crystallinity of DC-sputtered copper. At lower powers and as the thickness of the thin film decreases, so too does the size of the crystalline grains. Additionally, low-powered DC magnetron sputtering directly causes the formation of an amorphous phase in between well-defined crystals, forming a surface that expands the grain boundaries of the surrounding crystals. These boundaries then impede charge mobility, thus directly reducing the copper thin film's conductivity. Based on experimental results obtained in another study, the electronic properties of Cu thin films should approach those of bulk copper with a power of 3.5 W/cm^2 and a thickness of 300nm or more (Le et. al., 2009).

Section 3.2 ADHESIVE ATTACHMENT RESULTS

Attempting to solder a copper wire to the copper traces resulted in the traces melting entirely at 200°C , but resulted in minimal changes below 160°C . Notably, although the top copper layer melted when exposed to solder at 200°C , the chromium underlayer did not melt at any temperatures or under any conditions tested. Touching the clean solder to the trace resulted in no melting, indicating that the solder itself likely alloyed with the copper thin film, dramatically lowering its melting point (Fig. 3.2). However, even without the introduction of solder, the copper traces softened enough under heat above 160°C to allow mild prodding from the soldering iron to pull a significant amount of it away from the surface.

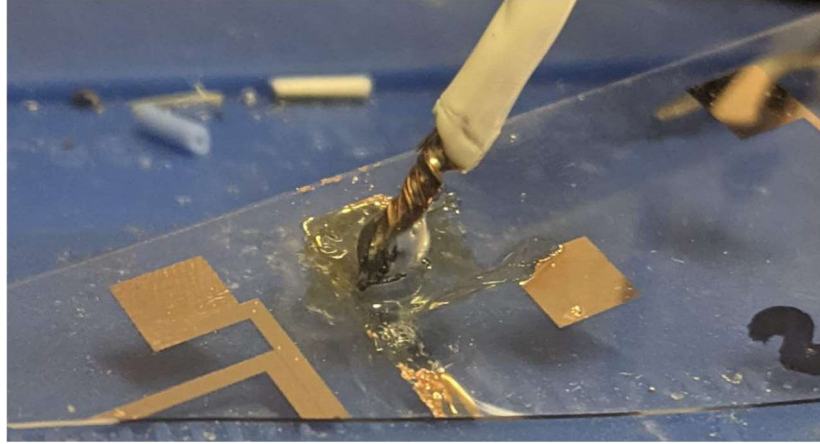


Figure 3.2: Sample 2S after the attachment of the 16 gauge copper wire using cuprate solder. The melting of the top copper layer is clearly visible in this image, as is the distinct beaded structure of the solder

The connection of the 16 gauge wire to the melted remains of the trace below was tenuous. Before resistance could be measured, the pressure of simply lifting and moving the wafer and attached wire was enough to break the two apart. This system clearly cannot withstand any amount of mechanical strain. This and the copper melting were both expected results: Sn-based solder alloys with copper thin films, effectively turning the trace below into solder and thus leaving nothing for the bead to bind to.

This happens due to the Cu-Sn binary system, where as temperatures reach approximately 200°C, the copper bonds to tin to form the ϵ - Cu_3Sn phase, which in turn has high solubility in the liquid phase of Sn. Then, as temperatures decrease, the binary compound settles into one of several possible solid alloy phases at room temperature, often including a solid η - Cu_6Sn_5 phase. This resultant phase is unavoidable unless a substantially different conducting solder is used, or unless the ratio of Cu to Sn in the solder-trace bond features considerably more copper than tin (Mookam et. al., 2018). Other conducting solders were not considered for this study due to their higher background compared to Sn-Ag solder and silver epoxy.



Figure 3.3: Sample 2S after the attachment of the 16 gauge copper wire using silver epoxy after one liquid nitrogen dunk cycle. Note the epoxy with no attached wires or leads on the bottom-leftmost test pad.

Regarding the silver epoxy, it formed a bond with the copper traces and maintained low resistances across the board. The precise values obtained will be discussed further when discussing the results of thermal cycling. Sample 2S was the first to be tested for this, with an excess of epoxy being used to attach the stranded 16 gauge wire to the test pad. Though not pretty, the result was a strong bond that could be used to hold up the sample, a property which was then used to subject it to a liquid nitrogen dunk test. Sample 1L was the next to have leads bonded using silver epoxy, this time with much thinner strands of copper extracted from the larger 16 gauge wire (Fig. 2.1). Once again, the resistance across each trace was unchanged initially, making it a promising candidate for cycling via the environment chamber.

The last two samples to have epoxy applied were samples 3 and 4. Although the initial goal was to attach multiple individual copper strands to several of their test pads as in sample 1L, sample 3 saw the strands attached to the top two pads of pair 14 and the bottom pad of trace 34L break away. The former saw mechanical failure of the copper itself, as the strands snapped into pieces shortly after the sample was moved. The latter saw a mechanical failure of the epoxy, as the strand slipped out of the epoxy without any damaged sustained by either (Fig. 3.4).



Figure 3.4: Pair 14 (left) and pair 34 (right) on sample 3. Note the lack of attached leads on the top two test pads of pair 14 and the bottom test pad of trace 34L.

Individual copper strands also caused difficulties in obtaining consistent measurements due both to their thinness and their tendency to pull on the epoxy on the surface when being pulled taut by the multimeter's leads. Both the difficulty of attachment and the difficulty of measurement of thin copper strands led to all further epoxy being applied with no leads, instead forming a test surface with a less variable resistance readout than the test pads themselves, thus giving more consistent measurements. These test pads were cured at 100°C for one hour in the environment chamber, then left overnight as it cooled naturally. As a result, the new corner traces cured as desired, but the epoxy deposited onto pairs 13 and 24 on sample 3 and 12, 13, 21R, 31R, and 32 on sample 4 was oxidized, becoming soft and yellow in coloration (Fig. 3.5).

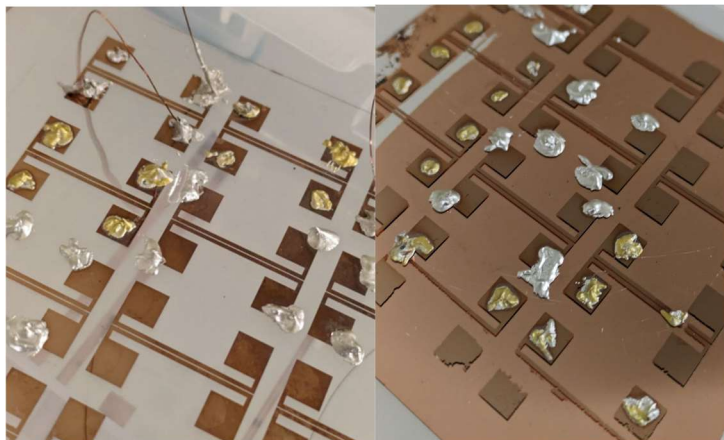


Figure 3.5 Oxidized epoxy visible on sample 3 (left) and sample 4 (right). The oxidized epoxy traces can be identified by their yellow coloration as compared to the normal silver coloration of the epoxy.

Section 3.3 THERMAL CYCLING RESULTS

Sample 2S was the first to undergo the liquid nitrogen dunk tests. These were performed as the sample was suspended by the silver epoxy-attached 16 gauge lead. These tests were performed without any intermittent resistance measurements, instead being used purely to test the epoxy's resilience under extreme conditions. Though it was more than strong enough to hold up the sample initially, after just three dunk cycles, the epoxy had already partially peeled away from the surface. After six dunk cycles, the epoxy peeled away entirely, with sample 2S falling entirely into the liquid nitrogen tank. Upon removal, the broken piece of silver epoxy was confirmed, with copper visibly having been pulled off from the surface trace (Fig. 3.6). After this, any measurements taken across any epoxy-laden traces on sample 2S returned either a discontinuous result, or a reading of approximately four M Ω , five orders of magnitude higher than the initial readings. This was confirmed on any trace with silver epoxy present, while the resistance of traces without any epoxy was perceptibly unchanged.

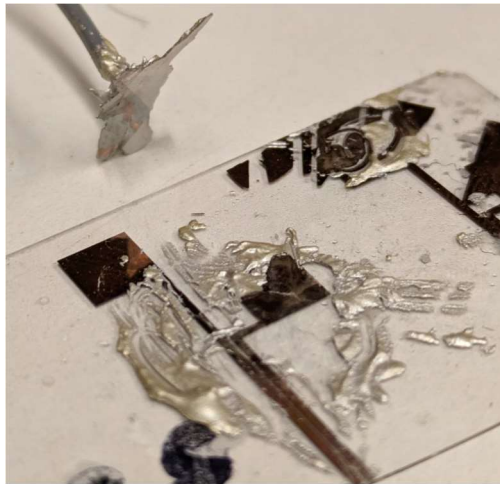


Figure 3.6: Sample 2S after six thermal cycles (bottom) and the 16 gauge copper wire coated in silver epoxy broken away (top). The copper visible on the bottom of the wire corresponds to visible blemishes in the trace below: Copper was apparently pulled off of the surface by the silver epoxy.

The copper that was melted on Sample 2S after the attempted solder connection test was notably completely removed by the first liquid nitrogen dunk test. Only the chromium interlayer remained afterwards, visually unaffected by that or any subsequent submersions (Fig. 3.7).

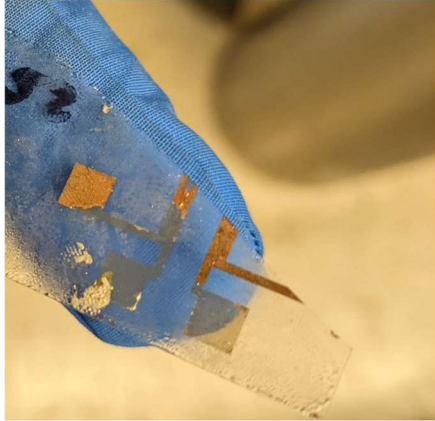


Figure 3.7: The solder test pads of sample 2S after one thermal cycle. Visibly, the opaque copper top layer has been pulled away while the translucent chromium thin interlayer is still present.

Next, Sample 1S was tested without any epoxy to isolate the failures of copper over chromium versus the failure of silver epoxy. This test was performed with low-temperature tape holding the sample as it was submerged into liquid nitrogen (Fig. 3.8). Like sample 2S, this attachment method failed after six cycles. Unlike the previous sample though, this time, the intermittent resistance measurements were taken on the testing pads between each cycle allowed for a more detailed view of the failure modes involved (Fig. 3.9).

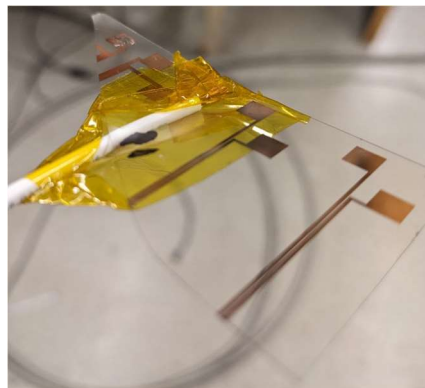


Figure 3.8: The tape applied to sample 1S. To the left of the 16 gauge white wire are control pads, measured only before and after all cycles. To the right are test pads, measured between every cycle. From left to right, they are numbered 1, 2, 3, 4, with traces 1 and 2 forming one pair, and 3 and 4 forming another.

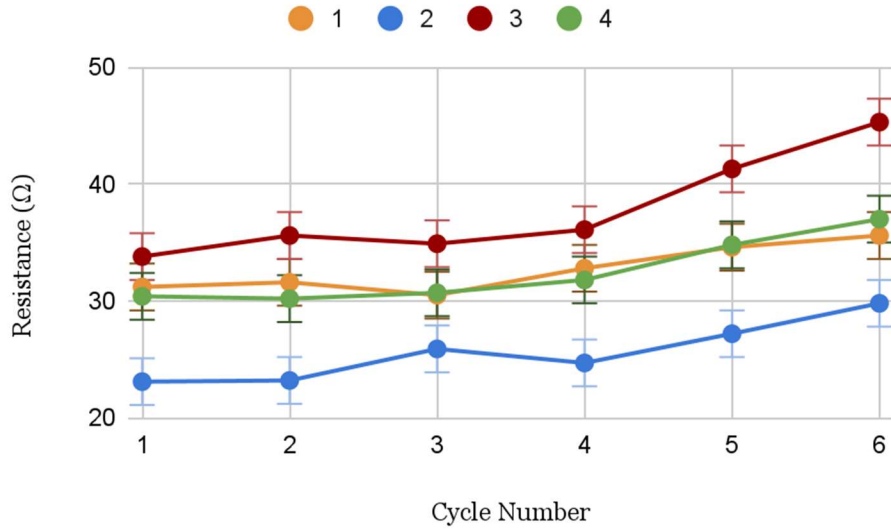


Figure 3.9: The resistance values of Sample 1S's four test traces

Over the course of the cycles, the stress caused by the thermal contraction of the tape and the pressure of the 16 gauge wire caused the sample to snap across the control traces, leaving only one intact. The test traces were unaffected by this, and the experiment showed a significant trend towards greater resistance between the test pad and the opposite end of the trace. This was not a trend mirrored by the control trace, which maintained a stable resistance of around 9Ω. Visually inspecting the two samples side-by-side revealed a likely cause of this observation: The process of touching the multimeter to the traces was causing tiny perforations within the trace, and the physical strain imposed by sudden submersion in liquid nitrogen was causing those perforations to be widened into gaps in the trace (Fig. 3.10).

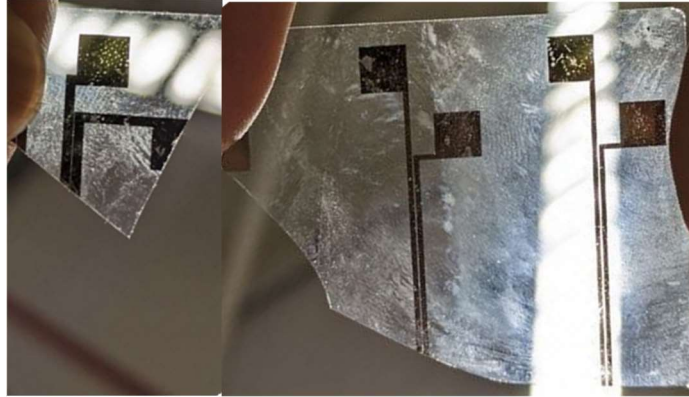


Figure 3.10 The surviving control trace (left) and test traces (right) of sample 1S after thermal cycling.

To identify the precise point of failure, and to mitigate physical stress imparted by full LN submersion, sample 1L was prepared with two test traces with copper strands attached to silver epoxy on the test pads, two test traces with no leads or epoxy, and four control traces as in sample 1S (Fig. 2.1). This time, the thermal cycling was performed in a controlled environment chamber that would lower it only to -100°C rather than bringing it down to the boiling point of nitrogen. Due to the more controlled nature of this experiment, there was no need for any tape or large wire to hold the sample in place.

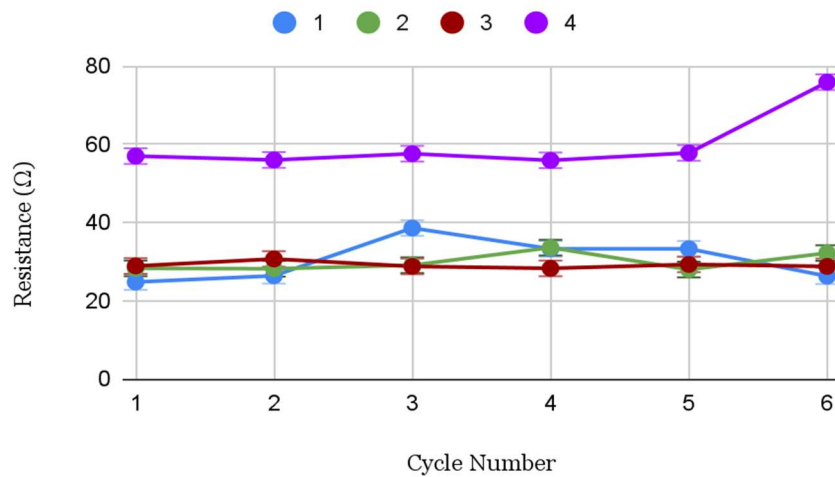


Figure 3.11: The resistance values of sample 1L's four test traces as labeled in Fig. 2.1

After the first cycle, the epoxy on traces 1 and 2 was already loose. After the second, the epoxy on trace 1 partially peeled away from the trace, bringing a substantial amount of copper with it. Pushing it back into position and leaving it overnight remedied this issue. However, after the third cycle, the epoxy peeled away entirely, bringing a substantial amount of the copper underlayer with it. The same happened in trace 2 after the fourth cycle. In both cases, after the epoxy peeled away, the space where it once was became either discontinuous or maintained a resistance on the order of $M\Omega$. Thus, all further resistance measurements were taken on the surviving copper around the missing epoxy.

The resistances across all traces were much more stable within this set of tests, with no statistically significant increase across cycles seen in all but trace 4. Being the longest trace, and also owing to a sizeable scratch along its trace visible in figure 3.12, it already had a significantly higher resistance than all other traces before any cycling. However, after the sixth and final cycle, the resistance of trace 4 increased dramatically as the scratch seemingly propagated, reducing the conductive surface of the trace to a vanishingly thin segment on one side. This mechanical damage corresponds to the sudden increase in trace 4's resistance (Fig. 3.11).



Figure 3.12: Sample 1L after all thermal cycling tests. The large damaged sections of copper are visible on traces 1 and 2 to the left. Traces 3 and 4, as well as all of the control traces, had small but visible gaps in the test pads compared to before any tests as seen in figure 2.1.

In the process of cycling and measuring the sample, a crack formed and propagated across the two leftmost control traces in figure 2.1. Of these, the leftmost trace remained mostly intact, with the middle-left trace being damaged enough to double its resistance. For the three surviving traces, however, the resistance consistently increased by around 2Ω . However, with a margin of error also around 2Ω , this result is interesting but may not be significant. Further thermal cycles would be needed to confirm whether this is a consistent result or merely a natural fluctuation in measurement.

After the thermal cycling of sample 1L, aside from the epoxy already peeled away from traces 1 and 2, visible damage at the point of contact with the multimeter leads was confirmed on all other traces, including the control traces (Fig. 3.12). Notably, the chromium underlayer in all cases appears to be undamaged on sample 1L, indicating a mechanical weakness in the Cu-Cr interface rather than the Cr-SiO₂ interface.

Section 3.4 SAMPLE 3 AND 4 RESULTS

The thermal cycling of samples 3 and 4, due to the variety of epoxy deposits and the number of test pads being investigated, is much more involved than the others. For the purposes of clarity and ease of discussion, each individual cycle's results will be addressed separately.

Before any thermal cycling was performed, the resistances of all test traces were measured to confirm that the epoxy had cured and to identify any other possible effects caused by the high-temperature curing process used on samples 3 and 4. All epoxy-laden traces were confirmed to have good connections, but exposed copper traces without epoxy exhibited rapidly fluctuating resistance values, the cause of which is yet to be determined. The results of these resistance tests are presented in tables 3-3 and 3-4, which can be compared to the initial resistances in tables 3-1 and 3-2.

An important feature of sample 4 to mention at this stage is the visible small blemishes in its traces. The edges of copper deposits on sample 4 are mostly jagged and rough, in contrast to the edges of copper deposits on sample 3, which are smooth. This indicates the large degree to which mechanical strain can pull away copper from the surface of quartz, which will only be exacerbated by thermal cycling, as will be shown below.

Table 3-3: The resistances in ohms of all test pairs on sample 3 after the application of silver epoxy and heat treatment at 100°C. The notations are the same as in Table 3-1. CTRL corresponds to control traces that were not measured between thermal cycles. Numbers in bold correspond to test traces without any epoxy. Highlighted numbers correspond to traces with oxidized epoxy.

| S. 3 | 1 | | 2 | | 3 | | 4 | |
|------|------|------|-----------------|-----------------|-----------------|-----------------|----------|----------|
| 1 | CTRL | CTRL | 25.0±1.1 | 26.7±1.3 | OL | 27.3±0.7 | 27.3±1.8 | 26.5±1.0 |
| 2 | CTRL | CTRL | 26.7±2.2 | 30.1±1.8 | <u>29.2±2.4</u> | 27.4±0.9 | 29.1±0.7 | 29.4±1.8 |
| 3 | CTRL | CTRL | 25.5±1.4 | 25.6±0.9 | <u>28.6±1.0</u> | <u>26.2±1.6</u> | 26.3±1.5 | 28.2±2.3 |

Table 3-4: The resistances in ohms of all test pairs on sample 4 after the application of silver epoxy and heat treatment at 100°C. The notations are the same as in Tables 3-1 and 3-3.

| S. 4 | 1 | | 2 | | 3 | | 4 | |
|------|----|----------|----------|----------|-----------------|----------|----------|----------|
| 1 | OL | OL | 27.6±1.1 | 27.1±1 | 30.4±0.8 | 34.4±2.1 | 29.7±1.1 | 31.5±1.9 |
| 2 | OL | 31.0±2.2 | 24.5±1.3 | 23.9±0.5 | 31.0±2.8 | 28.5±1.6 | CTRL | CTRL |
| 3 | OL | 43.6±1.8 | 46.1±2.1 | | <u>25.9±2.1</u> | 27.2±1.9 | CTRL | CTRL |

Comparing the results of tables 3-3 and 3-4 to those of tables 3-1 and 3-2, there's an apparent trend of the resistances of all test pads on sample 3 increasing by around 3Ω, with some, such as trace 22L, increasing by as much as 5Ω, and others, such as trace 34L, increasing by as little as 2Ω. Only the traces of pair 24 see no increase at all. Interestingly, this trend is not mirrored by sample 4, where many traces see an increased resistance of only 1Ω, and some, such as trace 12L, even show a decrease in resistance between tests. Samples 2S and 1L, which were cured at room temperature, did not see as significant of a rise in resistance, indicating that the heat treatment of samples 3 and 4 may have played a role.

Considering that the primary difference between the traces on samples 3 and 4 is the presence of a chromium interlayer in sample 4, this may indicate a feature of the Cu-Cr or Cr-SiO₂ interface that lowers trace integrity at higher temperatures as compared to the Cu-SiO₂ interface. Further testing would be required to confirm these results and identify the mechanism for this increase in resistance.

At this stage, the traces with oxidized epoxy seem to be outperforming those without, exhibiting fewer increases in resistance as compared to the initial sample with no epoxy, and in some cases even apparently decreasing the resistance of their corresponding trace. This trend would be reversed, however, once thermal cycling would begin.

After the first thermal cycle, a stress test was conducted using a set of tweezers to gently apply tension to each epoxy pad and pull it away from the surface. This was successful in all oxidized traces that did not go over the edges or corners of their respective test pads after the first thermal cycle as their resistances skyrocketed, in some cases becoming discontinuous, indicating a stark drop in their adhesion.

Comparing the removed epoxy pads from samples 3 and 4 reveals a notable distinction as well: Epoxy pads removed from sample 4 pulled away the entire copper layer they were attached to, indicating a failure occurring between copper and quartz. Epoxy pads removed from sample 3 often pulled up little if any copper, at times detaching from the surface and leaving a relatively undamaged and measurable test pad behind. In some cases, these pads pulled up small amounts of chromium and copper from the surface, indicating minor failures between copper, chromium, and quartz, and major, consistent failures between oxidized epoxy and copper (Fig. 3.13).

Additionally, on sample 3, both test pads on trace 14L, the top test pad on 14R, and both test pads on trace 34R came away entirely. In these cases, the entire copper layer, and in some cases the entire chromium layer, came away from the surface, indicating that when cured properly, silver epoxy is not as notable of a point of failure (Fig. 3.13).

In summation, mechanically speaking, a few consistent trends emerged from the first thermal cycling test:

- 1) Oxidized epoxy peeled away with minimal damage to sample 3
- 2) Oxidized epoxy peeled away with large amounts of damage to sample 4
- 3) Pristine epoxy peeled away with large amounts of damage, regardless of sample
- 4) Epoxy that made contact with quartz did not peel away, regardless of oxidization and regardless of which sample it was on.

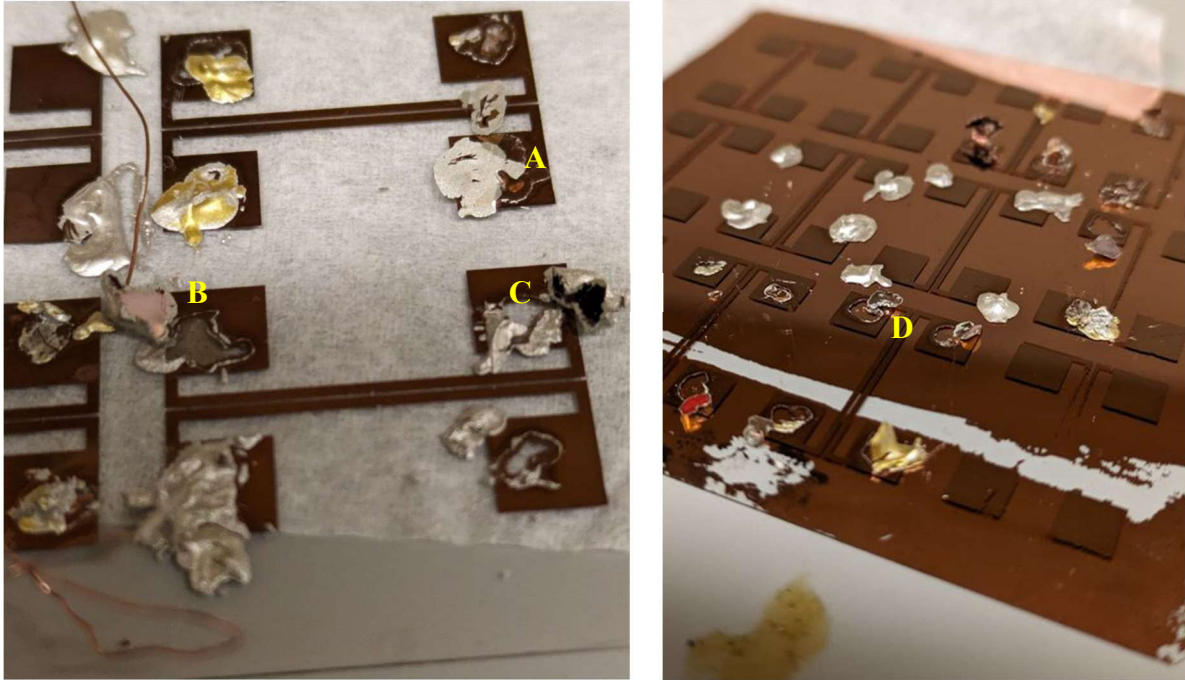


Figure 3.13: Examples of peeled away traces partway through the stress tests of sample 3 (left) and 4 (right) after the first thermal cycle. A) The undersides of oxidized epoxy pulled from pair 13 of sample 3. B) The underside of pristine epoxy pulled from trace 14L from sample 3. C) The underside of pristine epoxy pulled from trace 14L from sample 3. D) The underside of oxidized epoxy pulled from pair 12 from sample 4.

For all traces with removed epoxy, further resistance measurements were obtained by touching the leads of the multimeter to the remaining copper beneath where the epoxy had been removed from. If this was impossible or yielded a discontinuous result, then measurements were taken by touching the leads to the remaining copper around the same test pad that the epoxy was removed from. If this was still discontinuous, measurements were taken across the traces nearest the test pads. If this was still discontinuous, measurements were reported as discontinuous. For most of the measurements on sample 4, there was no visible damage to account for these discontinuities.

Table 3-5: The resistances in ohms of all test pairs on sample 3 after the first thermal cycle. The notations are the same as in Tables 3-1 and 3-3. Numbers highlighted in yellow correspond to traces with removed epoxy.

| S. 3 | 1 | | 2 | | 3 | | 4 | |
|------|------|------|-----------------|-----------------|-----------------|-----------------|-----------------|-----------------|
| 1 | CTRL | CTRL | 24.5±0.8 | 25.9±1.9 | OL | 27.7±0.8 | 183.4±4.8 | 26.4±1.3 |
| 2 | CTRL | CTRL | <u>27.9±0.9</u> | <u>32.9±3.6</u> | <u>28.9±0.7</u> | 28.4±1.2 | <u>31.7±1.1</u> | <u>30.0±1.6</u> |
| 3 | CTRL | CTRL | <u>26.3±2.3</u> | <u>25.9±2.3</u> | <u>32.1±1.5</u> | <u>27.4±1.1</u> | <u>31.6±1.1</u> | <u>26.4±3.3</u> |

Table 3-6: The resistances in ohms of test pairs on sample 4 after the first thermal cycle. The notations are the same as in Tables 3-1, 3-3, and 3-5. OL (D) corresponds to traces that became discontinuous due to physical damage.

| S. 4 | 1 | | 2 | | 3 | | 4 | |
|------|----|----|----------|--------|-----------------|--------|--------|------|
| 1 | OL | OL | OL (D) | OL | OL | OL | 33.5±3 | OL |
| 2 | OL | OL | 28.5±1.3 | OL (D) | 29.6±0.9 | OL | CTRL | CTRL |
| 3 | OL | OL | 62±7.5 | | <u>33.4±1.3</u> | OL (D) | CTRL | CTRL |

In order to identify which discontinuities were caused by damage or not, the multimeter was employed at several points along the trace itself. If there was a connection across a section of the trace greater than 10mm, it would indicate that the discontinuities were localized on the test pads, where damage is more common due to the frequent measurements. If there was no continuous connection except for when the leads of the multimeter were next to one another, it would indicate that there was no singularly isolated point of damage or imperfection, and that the discontinuity was fundamental to the trace itself. The results of this are seen in table 3-6.

Compared to previous tests, the increased resistance across most traces after the first thermal cycle is limited, being well within the margin of error for almost all cases. Notably, the epoxy on trace 23L of sample 4 was extremely soft and pliable, with a resistance that was decreasing with each measurement. Altogether, sample 3 fared relatively well in this cycle.

After the second thermal cycle, more sections of epoxy peeled away from the surface. However, in all cases, these pieces of epoxy were either part of the same test pad or the same trace as a piece from the previous thermal cycle, and thus tables 7 and 8 will not reflect these changes in terms of notation.

Table 3-7: The resistances in ohms of all test pairs on sample 3 after the second thermal cycle. The notations are the same as in Tables 3-1, 3-3, 3-5, and 3-6.

| S. 3 | 1 | | 2 | | 3 | | 4 | |
|------|------|------|-----------------|-----------------|-----------------|-----------------|-----------------|-----------------|
| 1 | CTRL | CTRL | 27.0±1.3 | 26.6±1.1 | OL | 30.1±1.3 | 33.3* | 28.4±1.5 |
| 2 | CTRL | CTRL | <u>28.3±0.8</u> | <u>29.5±1.1</u> | 29.5±2 | 27.7±1 | <u>29.8±0.4</u> | <u>33.5±1.8</u> |
| 3 | CTRL | CTRL | <u>27.5±1.2</u> | <u>26.6±1</u> | <u>36.6±1.6</u> | <u>28.7±1.3</u> | <u>29.7±0.6</u> | <u>27.5±1</u> |

Table 3-8: The resistances in ohms of all test pairs on sample 4 after the second thermal cycle. The notations are the same as in Tables 3-1, 3-3, 3-5, and 3-6.

| S. 4 | 1 | | 2 | | 3 | | 4 | |
|------|----|----|----------|--------|-----------------|--------|------|------|
| 1 | OL | OL | OL (D) | OL | OL | OL | OL | OL |
| 2 | OL | OL | OL | OL (D) | OL (D) | OL (D) | CTRL | CTRL |
| 3 | OL | OL | 75.6±0.9 | | <u>30.3±2.1</u> | OL (D) | CTRL | CTRL |

Trace 14L on sample 3 had three greatly varying yet consistent values across three different points on the test pad: In the chromium wake of the lifted epoxy, there was a measurement of around 17.9±0.7 MΩ. On the farthest surviving corners of the test pads, there was a measurement of around 610.4±1.6 Ω. On the nearest corners of the test pads, there was a measurement of around 33.3±2.2 Ω.

On the whole, the resistances across samples 3 and 4 are varying between thermal cycles, but apart from particular isolated instances, there is no remarkable trend towards increasing or decreasing resistance. Of particular note is the dramatic increase in discontinuous traces on

sample 4. Regardless of whether physical damage is to blame, the prevalence of discontinuous traces without chromium present versus the relatively stable traces on sample 3, with a present chromium interlayer, indicates a great success in the adhesive application of chromium as an interlayer compared to copper directly on quartz.

CONCLUSIONS

It is clear that the Cu-SiO₂ system breaks down electronically via compounding discontinuities not accounted for by physical damage over the course of multiple thermal cycles, indicating a shortcoming within the Cu-SiO₂ interface that becomes more and more prevalent the more the sample's temperature varies. Conversely, when exposed to low temperatures without external pressures such as dangling wires or physical contact with boiling liquid nitrogen, samples with chromium interlayers experience no significant setbacks in terms of physical damage or electronic conductivity

Regarding adhesives, considering copper thin films, silver epoxy remains the most promising candidate. However, this is not without its drawbacks: the mechanical strain caused by even individual copper strands has proven to be enough to detach epoxy from the copper surface below. Additionally, an improper ratio between resin and hardener within the silver epoxy has proven to be sufficient to cause the epoxy itself to lose adhesion rather than causing breakages within the metal layers in the chromium interlayer samples. If mixed with a proper ratio, cured properly, and attached partially to the quartz substrate, however, silver epoxy proves to be durable, temperature resistant, consistent in its resistivity, and it causes minimal, if any, damage to the layers beneath.

The behavior of the chromium interlayer is of some note, however. Given properly cured epoxy and significant amounts of stress, both the Cu-Cr interface and the Cr-SiO₂ interface have been observed to fail in the epoxy's stead, especially with leads attached. In light of this, future tests will be needed to determine the viability of other interlayers. Of particular note is Ti, which has a lower background rate than Cr by one order of magnitude, with a ²³²Th incidence rate on the order of 10⁻¹⁰ g/g, as opposed to Cr's rate on the order of 10⁻⁹g/g (Abgrall et. al., 2016).

Thus, further research will be required to identify the preferred interlayer between Cr and Ti for the Cu-SiO₂ system. Along with this, the next concern to address with regards to surface adhesives is the stress imparted by attached leads, as well as the tendency of leads to either break at the point of contact with epoxy or be pulled away from the cured epoxy with no damage sustained by either material.

Once both the interlayer and the adhesive measures have been identified, next will come the need to quantitatively measure important features of front-end circuitry, such as differential trace impedance across temperatures. Also of future interest is the mechanical and electronic integrity of plated-through-holes and through-quartz-vias, both of which suffer from physical damage-related failures due to accumulated thermal stresses (Fei et. al., 2020).

In short, the feasibility conclusions of this research open the door to many further advancements that can ultimately help facilitate the sensitivity goals of the nEXO collaboration.

REFERENCES

- Abgrall, N., Arnquist, I.J., Avignone III, F.T., Back, H.O., Barabash, A.S., Bertrand, F.E., Boswell, M., Bradley, A.W., Brudanin, V., Busch, M., Buuck, M., Byram, D., Caldwell, A.S., Chan, Y-D., Christofferson, C.D., Chu, P.-H., Cuesta, C., Detwiler, J.A., Dunmore, J.A., Efremenko, Yu., Ejiri, H., Elliott, S.R., Finnerty, P., Galindo-Uribarri, A., Gehman, V.M., Gilliss, T., Giovanetti, G.K., Goett, J., Green, M.P., Gruszko, J., Guinn, I.S., Guiseppe, V.E., Henning, R., Hoppe, E.W., Howard, S., Howe, M.A., Jasinski, B.R., Johnson, R.A., Keeter, K.J., Kidd, M.F., Kochetoi, O., Konovalov, S.I., Kouzes, R.T., LaFerriere, B.D., Leon, J., Loach, J.C., MacMullin, J., MacMullin, S., Martin, R.D., Massarczyk, R., Meijer, S., Mertens, S., Miller, M.L., Orrell, J.L., OShaughnessy, C., Overman, N.R., Poon, A.W.P., Pushkin, K., Radford, D.C., Rager, J., Rielage, K., Robertson, R.G.H., Romero-Romero, E., Ronquest, M.C., Schubert, A.G., Shanks, B., Shirchenko, M., Snavely, K.J., Snyder, N., Steele, D., Suriano, A.M., Tedeschi, D., Trimble, J.E., Varner, R.L., Vasilyev, S., Vetter, K., Vorren, K., White, B.R., Wilkerson, J.F., Wiseman, C., Xu, W., Yakushev, E., Yu, C.-H., Yumatov, V., Zhitnikov, I. (2016). The Majorana Demonstrator Radioassay program. *Nuclear Instruments and Methods in Physics Research Section A: Accelerators, Spectrometers, Detectors and Associated Equipment*, 828, 22–36. <https://doi.org/10.1016/j.nima.2016.04.070>
- Adhikari, G., Al Kharusi, S., Angelico, E., Anton, G., Arnquist, I. J., Badhrees, I., Bane, J., Belov, V., Bernard, E. P., Bhatta, T., Bolotnikov, A., Breur, P. A., Brodsky, J. P., Brown, E., Brunner, T., Caden, E., Cao, G. F., Cao, L., Chambers, C., Chana, B., Charlebois, A. S., Chernyak, D., Chiu, M., Cleveland, B., Collister, R., Czyz, A. S., Dalmasson, J., Daniels, T., Darroch, L., DeVoe, R., Di Vacri, L. M., Dilling, J., Ding, Y. Y., Dolgolenko, A., Dolinski, J. M., Dragone, A., Echevers, J., Elbeltagi, M., Fabris, L., Fairbank, D., Fairbank, W., Farine, J., Ferrara, S., Feyzbakhsh, S., Fu, S. Y., Gallina, G., Gautam, P., Giacomini, G., C. Gingras, Gillis W., Goeldi, D., Gornea, R., Gratta, G., Hardy, A. C., Harouaka, K., Heffner, M., Hoppe, W. E., House, A., Iverson, A., Jamil, A., Jewell, M., Jiang, S. X., Karelin, A., Kaufman, J. L., Kotov, I., Krücken, R., Kuchenkov, A., Kumar, S. K., Lan, Y., Larson, A., Leach, G. K., Lenardo, G. B., Leonard, S. D., Li, G., Li, S., Li, Z., Licciardi, C., Lindsay, R., MacLellan, R., Mahtab, M., Martel-Dion, P., Masbou, J., Massacret, N., McElroy, T., McMichael, K., Medina Peregrina, M., Michel, T., Mong, B., Moore, C. D., Murray, K., Nattress, J., Natzke, R. C., Newby, J. R., Ni, K., Nolet, F., Nusair, O., Nzobadila Ondze, C. J., Odgers, K., Odian, A., Orrell, L. J., Ortega, S. G., Overman, T. C., Parent, S., Perna, A., Piepke, A., Pocar, A., Pratte, J-F., Priel, N., Radeka, V., Raguzin, E., Ramonnye, J. G., Rao, T., Rasiwala, H., Rescia, S., Retière, F., Ringuette, J., Riot, V., Rossignol, T., Rowson, C. P., Roy, N., Saldanha, R., Sangiorgio, S., Shang, X., Soma, K. A., Spadoni, F., Stekhanov, V., Sun, L. X., Tarka, M., Thibado, S., Tidball, A., Todd, J., Totev, T., Triambak, S., M. Tsang, H. R., Tsang, T., Vachon, F., Veeraghavan, V., Viel, S., Vivo-Vilches, C., Vogel, P., Vuilleumier, J-L., Wagenpfeil, M., Wager, T., Walent, M., Wamba, K., Wang, Q., Wei, W., Wen, J. L., Wichoski, U., Wilde, S., Worcester, M., Wu, X. S., Wu, H. W., Wu, X., Xia, Q., Yan, W., Yang, H., Yang, L., Zeldovich, O., Zhao, J., Ziegler, T. (2021). Nexo: Neutrinoless double beta decay search beyond 10^{28} Year Half-life sensitivity. *Journal of Physics G: Nuclear and Particle Physics*, 49(1), 015104. <https://doi.org/10.1088/1361-6471/ac3631>

- Baima, J., Le, H.-L. T., Goniakowski, J., Noguera, C., Koltsov, A., & Mataigne, J.-M. (2020). Theoretical study of metal/silica interfaces: Ti, Fe, Cr and Ni on β -cristobalite. *Physical Chemistry Chemical Physics*, 22(37), 21453–21462. <https://doi.org/10.1039/d0cp03216f>
- Cui, Z., Chen, X., Fan, X., & Zhang, G. (2018). Interfacial properties of Cu/SiO₂ using a multiscale modelling approach in electronic packages. *2018 19th International Conference on Thermal, Mechanical and Multi-Physics Simulation and Experiments in Microelectronics and Microsystems (EuroSimE)*. <https://doi.org/10.1109/eurosime.2018.8369949>
- Fei, J.-B., Xu, T., Zhou, J.-Y., Ke, C.-B., & Zhang, X.-P. (2020). Interfacial crack initiation and delamination propagation in Cu-filled TSV structure by incorporating cohesive zone model and finite element method. *2020 IEEE 70th Electronic Components and Technology Conference (ECTC)*. <https://doi.org/10.1109/ectc32862.2020.00190>
- Le, M.-T., Sohn, Y.-U., Lim, J.-W., & Choi, G.-S. (2010). Effect of sputtering power on the nucleation and growth of Cu films deposited by Magnetron Sputtering. *MATERIALS TRANSACTIONS*, 51(1), 116–120. <https://doi.org/10.2320/matertrans.m2009183>
- Mookam, N., Tunthawiroon, P., & Kanlayasiri, K. (2018). Effects of copper content in Sn-based solder on the Intermetallic Phase Formation and growth during soldering. *IOP Conference Series: Materials Science and Engineering*, 361, 012008. <https://doi.org/10.1088/1757-899x/361/1/012008>
- Shan, T.-R., Devine, B. D., Phillpot, S. R., & Sinnott, S. B. (2011). Molecular dynamics study of the adhesion of Cu/SiO₂ interfaces using a variable-charge interatomic potential. *Physical Review B*, 83(11). <https://doi.org/10.1103/physrevb.83.115327>
- Yang, L., Yang, X., Gao, F., Guan, Y., Wan, R., & Wang, P. (2023). Enhanced adhesion of copper films on fused silica glass substrate by plasma pre-treatment. *Materials*, 16(14), 5152. <https://doi.org/10.3390/ma16145152>